7th Annual International IEEE EMBS Conference on Neural Engineering
Montpellier, France, 22 - 24 April, 2015

Frequency-Dependent Simulation of Volume Conduction in a Linear Model of the Implanted Cochlea*

Chidrupi Inguva, Paul Wong, Andrian Sue, Alistair McEwan, and Paul Carter

Abstract— **Volume conduction models of the implanted cochlea are useful tools for investigating cochlear implant function. To date, however, all existing models have assumed that the tissues of the cochlea are purely resistive, despite evidence to the contrary. In this paper, a preliminary attempt to incorporate frequency-dependent effects is made using a simple, extruded finite element model of the cochlea. It was found that resistive and dispersive formulations exhibited marked differences in the pattern of current flow, especially later in the phase. The scala tympani response remained largely resistive as per published experimental evidence. However, injected current was also diverted away from higher impedance bone and neural tissue towards lower impedance pathways, particularly the cerebrospinal fluid in the modiolus. Further investigation of these effects is warranted to better understand these differences and how they might affect existing models of neural excitation.**

I. Introduction

Computational models of the implanted cochlea [1]–[7] have been used to investigate the function of cochlear implants (CIs), which can restore hearing perception in individuals with sensorineural hearing loss. All volume conduction models (VCMs) of the implanted cochlea to date have assumed that the tissues are purely resistive as a first approximation in order to invoke the quasi-static condition [8]. Experimental evidence showing that phase lag within the scala tympani is negligible [9] is usually cited as justification. However, it is known that biological tissues are not purely resistive due to the presence of proteins and cell membranes [10]. Tissues whose dielectric properties have been measured demonstrate that both conductivity and permittivity vary with frequency [11]. Aside from its fluid spaces, the cochlea is largely comprised of bone and nerve, both of which have well-documented capacitive effects [10]–[13]. Combined with the use of square-shaped current pulses in CI stimulation, it is likely that capacitive effects could play a larger role than is currently expected.

The quasi-static assumption is only applicable if:

$$\omega\varepsilon_0\varepsilon_r/\sigma << 1, \quad (1)$$

where ω is the angular frequency of the current source, ε_0 is the permittivity of free space, ε_r is the relative permittivity of the tissue, and σ is the conductivity of the tissue [8]. This condition may not hold for some of the tissue types included in VCMs of the cochlea.

Table 1 calculates the quasi-static criterion for cochlear tissues at 10 kHz, the fundamental frequency used in these simulations. The conductivity values are specific to the cochlear tissues. Although the frequency at which they were measured ranged from 1–1000 Hz [14], most tissue conductivities vary only slightly at low frequencies [11] so these numbers are the best available estimate for the conductivities at 10 kHz. The relative permittivity values for selected tissues were sourced from Hasgall et al. [15], whose online database is the most comprehensive source of dielectric tissue properties at the time of writing. The estimated criterion values are generally less than one at the fundamental frequency, but for some tissues, particularly nerve, it is not substantially less. Also note that the criterion is proportional with frequency and will increase to well over one at higher harmonics, suggesting that time-dependent effects are relevant and should be incorporated. It is

TABLE I. Material Properties & the Quasi-static Criterion at the Fundamental Frequency

Material	Conductivity (S/m)	Relative Permittivity	$\omega\varepsilon_0\varepsilon_r/\sigma$
Bone	0.0204[a]	521.64[a]	0.014
Nerve	0.0424[a]	35569[a]	0.467
CSF	2[a]	109[a]	3.03×10^{-5}
Perilymph	1.42[b]	1	3.92×10^{-7}
Endolymph	1.67[b]	1	3.33×10^{-7}
Blood	0.7[a]	5248.2[a]	4.17×10^{-3}
Spiral ligament	1.67[c]	1	3.33×10^{-7}
Stria vascularis	5.30×10^{-3} [c]	1	1.05×10^{-4}
Organ of Corti	1.20×10^{-2} [c]	1	4.64×10^{-5}
Reissner's membrane	9.80×10^{-5} [b]	1	5.68×10^{-3}
Basilar membrane	1.25×10^{-2} [b]	1	4.45×10^{-5}
Silicone	1×10^{-7}	1	5.56
Platinum	1×10^{8}	1	5.56×10^{-15}

Tissues without reported relative permittivity values were assumed to be purely resistive.

a. Obtained from Hasgall *et al.* [15] at the fundamental frequency (10 kHz)
b. From Finley *et al.* [2]
c. From Frijns *et al.* [3]

*This research was supported in part by the ARC through a Linkage Scheme (LP0776938).

C. Inguva and A. McEwan (phone: +61 2 9351 7256; e-mail: alistair.mcewan@sydney.edu.au) are with the School of Electrical Engineering, University of Sydney, Sydney, NSW 2006 Australia.

P. Wong (e-mail: paul.wong@sydney.edu.au) and A. Sue are Ph.D. candidates with the School of Aerospace, Mechanical and Mechatronic Engineering, University of Sydney, Sydney, NSW 2006 Australia. They are each recipients of an Australian Postgraduate Award. P. Wong is also the recipient of a University of Sydney Merit Award.

P. Carter is in Implants Development at Cochlear Limited, Sydney, NSW 2109 Australia (e-mail: pcarter@cochlear.com).

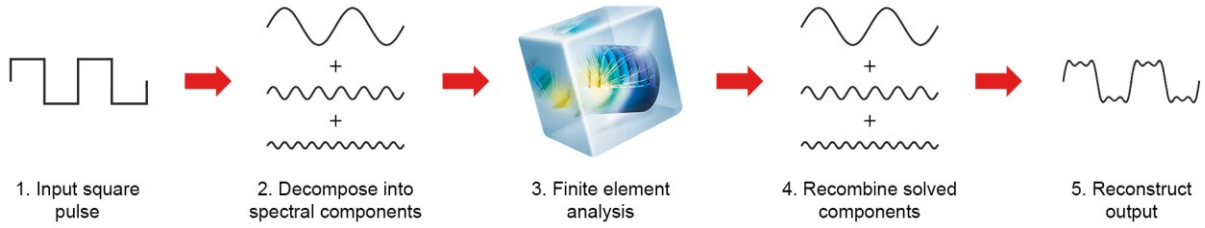

Figure 1. The solution process involved decomposing a square biphasic current pulse in the time domain into its spectral components via a Fourier transformation. Each frequency was analysed in COMSOL Multiphysics, and the outputs recombined to obtain the corresponding transient response.

hypothesized that the field quantities in Rosenthal's canal, within which lie the spiral ganglion cells, could show significant differences between resistive and dispersive formulations, and if that were the case, neural excitation models may need to be adjusted to account for this effect.

In this study, capacitive effects were incorporated in an anatomically detailed VCM of the implanted cochlea in order to gain some insight into how the current pathways might change during a stimulation pulse. This will provide some guidance for future modeling efforts.

II. Method

A. Model Development

The finite element (FE) model used in this study was based on earlier work by Wong *et al.* [7]. A histological cross-section through one turn of the human cochlea was segmented into 11 tissue types, as listed in Table 1, and extruded to form a linear model. Compared to the previous iteration, the segmentation has been updated slightly to aid visualization and improve accuracy. The overall length of the model was increased to encompass five electrode contacts.

Mesh generation was performed in ICEM CFD (ANSYS Inc, Canonsburg PA, USA). This allowed a computer-aided design (CAD) model of the array to be easily inserted and provided a high degree of control over element sizing as well as a high quality mesh. The final volume mesh consisted of 813,816 nodes and 4,765,154 elements, and was imported into COMSOL Multiphysics (COMSOL AB, Stockholm, Sweden) for FE analysis.

For both of the following scenarios, a square-shaped biphasic pulse (50 μs per phase) with an amplitude of 1 mA was delivered at the middle electrode contact. The first (cathodic) phase was of primary interest, since this is the phase primarily involved in neuronal recruitment. The bottom surface, corresponding to the basal aspect of the auditory nerve trunk, was grounded to represent the mono-polar return pathway [1].

B. Resistive Simulation

The resistive case was set up to replicate existing models that assume purely resistive cochlear tissues. Under this simplification, the permittivity for all tissues was assigned as that of free space. The conductivities used were the commonly cited cochlea-specific values from existing models (see Table 1), with the exception of bone, nerve, CSF, and blood, for which frequency-dependent values were available [15]. For these tissues, the conductivity at the fundamental frequency was used.

In the purely resistive formulation, the calculated field quantities are synchronous with the rise and fall of the input current [8]. This allows the quasi-static assumption to be applied, and the simulation to be run as a stationary analysis with a 1 mA constant current source at the active electrode.

C. Dispersive Simulation

To model the dispersive field quantities, frequency-dependent material properties [15] were required. Unfortunately, these properties have not been measured for cochlear-specific tissues, so only selected tissues with available comparable data (bone, nerve, CSF, and blood) were changed; the other tissues were left as they were in the resistive case. For bone, nerve, CSF, and blood, both conductivity and relative permittivity values over the entire available frequency range were assigned.

The setup and analysis process was a simplified version of that used by previous studies [13], [16] and is summarized in Fig. 1. Instead of considering the pulse in the time domain, its fundamental frequency and first 500 harmonics were weighted and combined as an analytical function in COMSOL, representing a discrete Fourier transformation of the current input. A frequency domain simulation was then performed on the system, sweeping from zero to 10 MHz. This allowed frequency-dependent properties to be accounted for in the analysis. The outputs from each spectral component were then recombined in MATLAB (The Mathworks, Inc., Natick MA, USA) to obtain the transient response. The time domain was preferred over the frequency domain because it provided a more intuitive representation of the dynamics in the system.

D. Model Outputs

The outputs of interest were current density over the duration of the pulse, evaluated at the mid-plane of the model, the direction of current flow, as shown by streamline plots, with seeding points spread over a regular quadratic grid on the surface of the stimulating electrode, and the activation function [17] along projected nerve fibers.

III. Results

The transient responses for both the resistive and dispersive formulations are plotted for points in the CSF (Fig. 2A), the scala tympani (Fig. 2B), Rosenthal's canal (Fig. 2C), and the lateral wall (Fig. 2D). The scala tympani

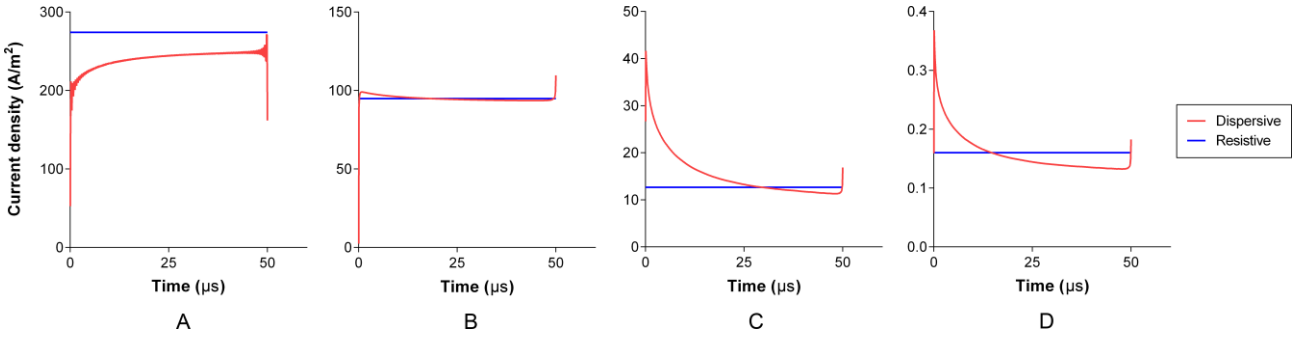

Figure 2. Current density at (A) the CSF, (B) the scala tympani, (C) Rosenthal's canal, and (D) the lateral wall at the centre plane over the duration of the pulse for the resistive (blue) and dispersive (red) cases. Note the difference in scales for each point. The scala tympani behaviour is predominantly resistive, in line with the findings of Spelman [9]. Current density is significantly higher for the time dependent case in Rosenthal's canal at the start of the pulse. The high relative permittivities of nerve and bone tissue mean that they experience the largest percentage change over time.

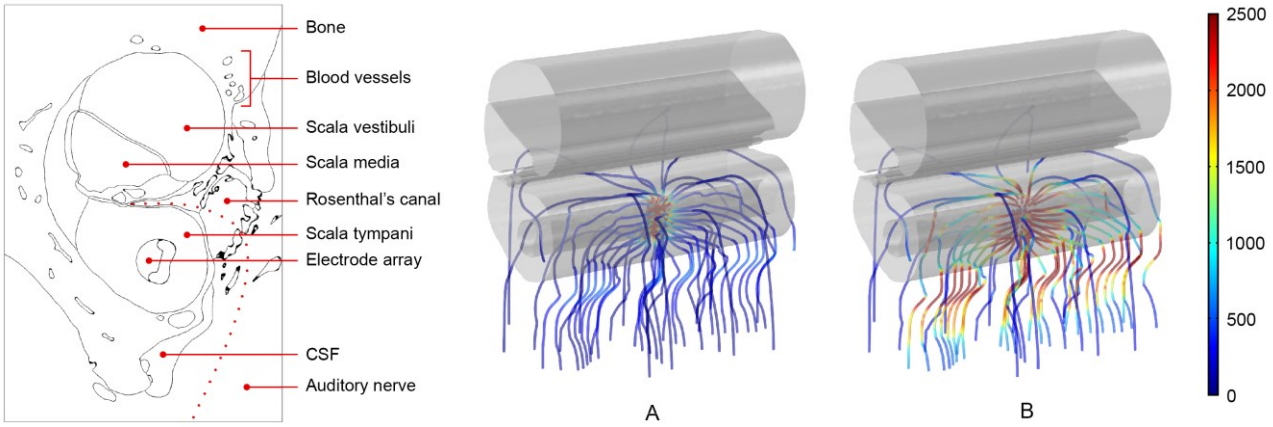

Figure 3. Medial view of the current density streamlines for (A) the resistive case and (B) the dispersive case at the fundamental frequency. Main tissues labelled in the cross section on the left; dotted line shows the projected trajectory of the nerve fibre used for calculating the activation function. The legend on the right measures current density in amps per meter squared (A/m^2). Current spread along the scala tympani can be seen in both cases. The dispersive case shows substantially higher current density in the pocket of CSF adjacent to the nerve.

exhibits largely resistive behavior, which corresponds with the experimental findings of Spelman [9]. At the same time, current density in the CSF pocket increases over the duration of the pulse, while both the spiral ganglion and the lateral wall experience a reduction. Overall current is conserved despite the differences in spatial and temporal distribution.

Fig. 3A and 3B show the direction of current flow for the resistive and dispersive cases respectively. The perilymphatic and endolymphatic spaces are shown in grey to provide some spatial context. In both plots, much of the current leaving from the edges of the electrode pad flow longitudinally through the scala tympani, while current from more central portions of the electrode surface flow towards the neural structures. The main difference between the two formulations is the magnitude of current density, which is significantly more concentrated in the pocket of CSF adjacent to the nerve trunk under the dispersive formulation.

A comparison of the discrete second derivative of voltage along the nerve fibers (representing the activation function) for both the resistive and dispersive formulations is shown in Fig. 4. It appears that the addition of capacitive effects causes pronounced fluctuations along each fiber relative to the purely resistive case. The values are highest in the center of the model and increase again towards the lateral margins.

IV. Discussion

The results of this study suggest that the quasi-static assumption does not hold for models of the implanted cochlea. Spelman's findings of minimal phase lag are only applicable to measurements within the scala tympani, where injected current has yet to pass through any dielectric tissues, and it is incorrect to extend this assumption to the entire domain. Charge storage effects in tissues beyond the scala tympani vary the electric field as time progresses throughout the stimulation pulse. Currents are higher earlier in the pulse in neural tissue because it stores significant charge due to its high permittivity. Current paths are redirected through low impedance tissues such as CSF. This has implications for VCMs that are coupled with neural excitation models, since these use the spatial distribution of the electric field as input to determine action potential generation [17]. The variable current density (Fig. 2C) suggests that purely resistive models may be insufficient to correctly predict the amount of charge delivered to neural tissues. Overall, these differences indicate that dispersive effects may be one reason why *in silico* predictions do not consistently match *in vivo* measurements, even with ideal data for comparison and validation [5].

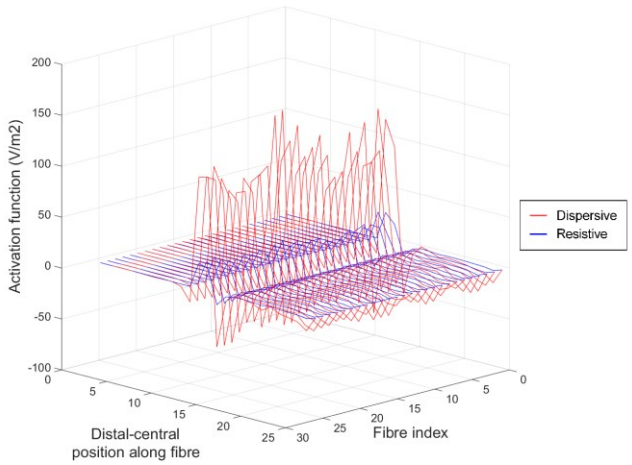

Figure 4. Activation function along the nerve fibres. The dispersive formulation shows similar trends to the resistive case, but with more pronounced fluctuations along each fibre. The limited physical scope of the model appears to prevent monotonic drop off away from the center.

As with other computational studies, the development of this model was dependent on a number of simplifications which may have a bearing on these results. First and most relevant to this study was that frequency-dependent dielectric properties were not available for all of the modeled tissues. Hasgall's database [15] only includes general bodily tissues, and the major tissue types likely to be involved in current conduction within the cochlea have been modeled with dielectric values. Unfortunately, data for cochlear-specific tissues are not currently available, and ideally a complete description of all cochlear tissues would be included.

While the geometry used was highly detailed in terms of the number and appearance of the cochlea tissues, the extruded shape fails to account for the true, spiraling nature of the cochlear anatomy, and the limited physical scope raises some questions over the accuracy of the imposed boundary conditions. Likewise, the increase in peak activation function laterally is likely due to these artificial constraints. Nevertheless, it is expected that similar trends would be demonstrated in models with more realistic geometries since the main consideration is the difference in material properties.

Lastly, it is worth noting that neural membranes only behave linearly below threshold and start to exhibit non-linear effects as levels approach threshold [17]. This may affect the validity of superimposing the harmonic results in regions of neural tissue near the stimulating electrode.

V. Conclusion

The study was a successful first attempt at incorporating frequency-dependent effects in a VCM of the implanted cochlea. A disparity was revealed between resistive and dispersive formulations of the model, and the data indicate that the quasi-static assumption is not valid for electric models of the cochlea. It is recommended that these effects are further explored in future modelling efforts. Extensions to the study are already planned, including a dynamic visualization of the current paths over the duration of the pulse, and an analogous analysis on a validated model of the guinea pig cochlea featuring true 3D anatomy.

Acknowledgment

The authors would like to thank Qing Li from the School of Aerospace, Mechanical and Mechatronic Engineering at the University of Sydney for providing the computational resources required to undertake this project.

References

[1] G. Girzon, "Investigation of current flow in the inner ear during electrical stimulation of intracochlear electrodes," Master's thesis, Dept. of Electrical Engineering and Computer Science, Massachusetts Institute of Technology, 1987.

[2] C.C. Finley, B.S. Wilson, and M.W. White, "Models of neural responsiveness to electrical stimulation," in *Cochlear implants: models of the electrically stimulated ear*, J.M. Miller, Springer-Verlag, 1990, pp. 55–96.

[3] J.H.M. Frijns, S.L. De Snoo, and R. Schoonhoven, "Potential distributions and neural excitation patterns in a rotationally symmetric model of the electrically stimulated cochlea," *Hearing research*, vol. 87(1-2), pp. 170–186, 1995.

[4] T. Hanekom, "Three-dimensional spiraling finite element model of the electrically stimulated cochlea," *Ear and hearing*, vol. 22(4), pp. 300–315, 2001.

[5] D.M. Whiten, "Electro-anatomical models of the cochlear implant," Ph.D. dissertation, Massachusetts Institute of Technology, 2007.

[6] J.H.M. Frijns, R.K. Kalkman, and J.J. Briaire, "Stimulation of the facial nerve by intracochlear electrodes in otosclerosis: a computer modeling study," *Otology & Neurotology*, vol. 30(8), pp. 1168–1174, 2009.

[7] P. Wong, Q. Li, and P. Carter, "Incorporating vascular structure into electric volume conduction models of the cochlea," presented at the IEEE EMBS Conference on Biomedical Engineering and Sciences, Langkawi, Malaysia, December, 2012.

[8] R. Plonsey and D.B. Heppner, "Considerations of quasi-stationarity in electrophysiological systems," *Bulletin of Mathematical Biophysics*, vol. 29, pp. 657–664, 1967.

[9] F.A. Spelman, B.M. Clopton, and B.E. Pfingst, "Tissue impedance and current flow in the implanted ear: Implications for the cochlear prosthesis," *The Annals of otology, rhinology & laryngology. Supplement*, vol. 98, pp. 3–8, 1982.

[10] S. Grimnes and Ø.G. Martinsen, *Bioimpedance and bioelectricity basics*, London, UK, Academic Press, 2000.

[11] S. Gabriel, R.W. Lau, and C. Gabriel, "The dielectric properties of biological tissues: III. Parametric models for the dielectric spectrum of tissues," *Physics in medicine and biology*, vol. 41, p. 2271, 1996.

[12] P.A. Williams and S. Saha, "The electrical and dielectric properties of human bone tissue and their relationship with density and bone mineral content," *Annals of Biomedical Engineering*, vol. 24, pp. 222–233, 1996.

[13] C.R. Butson and C.C. McIntyre, "Tissue and electrode capacitance reduce neural activation volumes during deep brain stimulation," *Clinical Neurophysiology*, vol 116, pp. 2490–2500, 2005.

[14] D. Strelioff, "A computer simulation of the generation and distribution of cochlear potentials," *The Journal of the Acoustical Society of America*, vol. 54(3), pp. 620–629, 1973.

[15] P.A. Hasgall, E. Neufeld, M.C. Gosselin, A. Klingenböck, and N. Kuster, "IT'IS Database for thermal and electromagnetic parameters of biological tissues," Version 2.5, August 1st, 2014. www.itis.ethz.ch/database

[16] C.A. Bossetti, M.J. Birdno, and W.M. Grill, "Analysis of quasi-static approximation for calculating potentials generated by neural stimulation," *Journal of Neural Engineering*, vol. 5, pp. 44–53, 2008.

[17] J.P. Reilly, *Applied Bioelectricity: From Electrical Stimulation to Electropathology*. New York, NY: Springer-Verlag, 1998, pp. 105–147.